Vol 17 No 3, March 2008
1674-1056/2008/17(03)/1034-07
Chinese Physics B
© 2008 Chin. Phys. Soc.
and IOP Publishing Ltd

Vertical rotation effect on turbulence characteristics in an open channel flow*

Zou Li-Yong(邹立勇)[a)†], Bai Jing-Song(柏劲松)[a)], Li Bu-Yang(李步阳)[b)],
Tan Duo-Wang(谭多望)[a)], Li Ping(李 平)[a)], and Liu Cang-Li(刘仓理)[a)]

[a)] *Laboratory for Shock Wave and Detonation Physics Research, Institute of Fluid Physics, China Academy of Engineering Physics, Mianyang* 621900, *China*

[b)] *General Electric Hydro Equipment Asia Co. Ltd., Hangzhou* 311231, *China*

(Received 16 April 2007; revised manuscript received 7 August 2007)

This paper solves the three-dimensional Navier–Stokes equation by a fractional-step method with the Reynolds number Re_τ=194 and the rotation number N_τ=0–0.12. When N_τ is less than 0.06, the turbulence statistics relevant to the spanwise velocity fluctuation are enhanced, but other statistics are suppressed. When N_τ is larger than 0.06, all the turbulence statistics decrease significantly. Reynolds stress budgets elucidate that turbulence kinetic energy in the vertical direction is transferred into the streamwise and spanwise directions. The flow structures exhibit that the bursting processes near the bottom wall are ejected toward the free surface. Evident change of near-surface streak structures of the velocity fluctuations are revealed.

Keywords: vertical rotating open channel flow, turbulence statistics, flow structure
PACC: 4725

1. Introduction

Rotating turbulent flows are widely encountered in atmospheric and astrophysical applications. In those flows, the rotational-induced additional body forces, i.e. centrifugal and Coriolis forces, make that the momentum mechanism becomes more complicated. Thus, a physical understanding of the turbulent flow in rotating frame is highly desired. On the other hand, the structure of turbulence is a key factor to reveal more fundamental knowledge of the interaction of turbulence with the surface.[1,2] Usually, the basic flow field for investigation of rotating flows with a free surface is a rotating shear flow in an open channel. Investigation of turbulent open channel flow subjected to the vertical rotation is quite different from that in widely studied spanwise rotating channel flow. Since mean vorticity component is perpendicular to the vertical rotating axis, turbulence is sensitive to the vertical rotation. Thus, the absolute mean flow deviates from the streamwise direction. The statistical coherent structures are verified to be more sensitive to the Coriolis force effect induced by the vertical rotation.[3] Currently, numerical investigations on the rotating channel flow mainly focus on the spanwise rotating flow. Little work for the vertical rotating open channel flow has been performed. However, understanding the effects of rotation in the vertical rotating open channel flow is an important issue because any model aimed at predicting the turbulence statistics should reproduce the essential features of this canonical situation. In this study, direct numerical simulation approach is used to calculate vertical rotating turbulent open channel flow. The motivation is to investigate the turbulence behaviours subjected to system rotation.

2. Mathematical formulations

2.1. Governing equations

The Navier–Stokes equation is used for direct numerical simulation of fully developed turbulent channel flow in a vertical rotating system. To nondimensionalize the governing equation, the wall friction velocity u_τ is used as the velocity scale, the channel depth h as the length scale. Then, the governing equations are given as

$$\frac{\partial u_i}{\partial x_i} = 0, \tag{1}$$

*Project supported by the National Natural Science Foundation of China (Grant Nos 10772166 and 10672151), and the Foundation of China Academy of Engineering Physics (Grant No 20050104).
†Corresponding author. E-mail: liyong.zou@gmail.com

$$\frac{\partial u_i}{\partial t}+\frac{\partial}{\partial x_j}(u_iu_j) = -\frac{\partial p}{\partial x_i}+\delta_{1i}+\frac{1}{\mathrm{Re}_\tau}\frac{\partial^2 u_i}{\partial x_j\partial x_j}-N_\tau\varepsilon_{ijk}\frac{\Omega_j}{|\Omega|}u_k, \quad (2)$$

where the normalized parameters are defined as $\mathrm{Re}_\tau = u_\tau h/\nu$ and $N_\tau = 2\,|\Omega|\,h/u_\tau$, with ν being the kinematic viscosity and Ω the angular speed of rotating frame.

As shown in Fig.1, the turbulent flow is driven by a constant streamwise pressure gradient. At the bottom wall $y = 0$, no-slip and no-penetration velocity conditions are imposed. Assuming the free surface being in the absence of surface deformation, we find that the boundary conditions applied at $y = 1$, are given by

$$v = 0, \quad \frac{\partial u}{\partial y} = \frac{\partial w}{\partial y} = 0. \quad (3)$$

The flow field is assumed to be statistically homogeneous in the streamwise and spanwise directions. Thus, periodic boundary conditions are employed in both the directions.

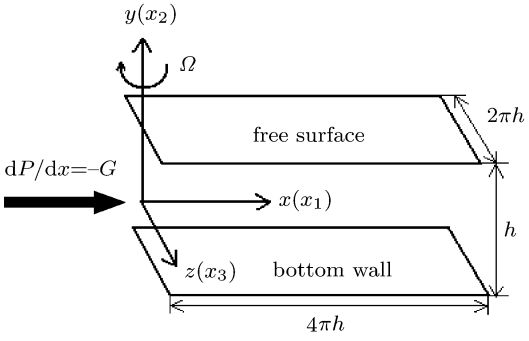


Fig.1. Sketch of the vertical rotating open channel flow. Here, G represents a positive number.

2.2. Solutions of vertical rotating laminar open channel flow

In the laminar flow of a vertical rotating open channel, the streamwise and spanwise velocity components satisfy the governing equations deduced by Ekman for wind-driven laminar flow above a horizontal plane subjected to earth's rotation, which can be written as

$$N_\tau U = \frac{1}{\mathrm{Re}_\tau}\frac{\mathrm{d}^2W}{\mathrm{d}y^2}, \quad (4)$$

$$-N_\tau\left(W+\frac{1}{N_\tau}\right) = \frac{1}{\mathrm{Re}_\tau}\frac{\mathrm{d}^2U}{\mathrm{d}y^2}. \quad (5)$$

According to boundary condition described in subsection 2.1, the solution for Eqs.(4) and (5) can be obtained as

$$U(y) = \mathrm{Im}(f(y)), \quad (6)$$

$$W(y) = Re(f(y)) - \frac{1}{N_\tau}, \quad (7)$$

where $f(y) = A(\mathrm{e}^{ky}+\mathrm{e}^{-ky})$, $A = (N_\tau(1+\mathrm{e}^{2k}))^{-1}$ and $k = (1-i)\sqrt{\mathrm{Re}_\tau N_\tau/2}$ and $\mathrm{Re}(f(y))$ and $\mathrm{Im}(f(y))$ denote the real and imaginary part of $f(y)$ respectively.

The streamwise and spanwise velocities from Eqs.(6) and (7) are shown in Fig.2. It is observed that U decreases sharply as N_τ increases and even tends to zero in the near-surface region. As for the spanwise velocity W, however, the Coriolis force augments it when N_τ is small and damps it obviously at strong N_τ case. Thus, it is reasonable that in this study the rotation number N_τ is chosen as from 0 to 0.12 to examine the rotating effect.

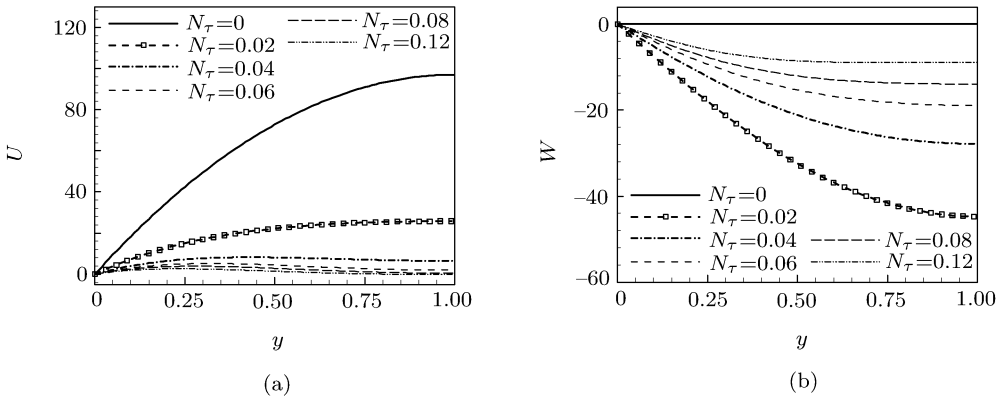


Fig.2. Distributions of the velocity for laminar flow in the vertical rotating open channel: (a) streamwise and (b) spanwise component.

3. Numerical methods

To solve Eqs.(1) and (2), spatial derivatives are discretized by a second order central difference. Time advancement is carried out by the semi-implicit scheme using the Crank–Nicolson scheme for the viscous terms and the three-stage Runge–Kutta scheme for the convective terms.

In this study, the Reynolds number is 194. The size of computational domain is $4\pi h \times 2\pi h \times h$ with the corresponding grid number 193×193×193 in the streamwise, spanwise and vertical directions, respectively. Along both the streamwise and spanwise directions, the grid is uniform. However, in the vertical direction, to increase the grid resolution near the free surface and the bottom wall, respectively, the mesh is stretched following the transformation.[4]

It is worthwhile to mention that the performance and reliability of the numerical method used in this study have been verified extensively.[5,6] Furthermore, extensive validations have been undertaken in our previous work.[7−11] Thus, it can be confirmed that numerical methods are reliable for the prediction of turbulence characteristics in the vertical rotating open channel.

4. Results and discussion

4.1. Turbulence statistics

The mean velocity in the streamwise and spanwise directions is calculated. However, as N_τ increases, the change tendency of $< u >$ and $< w >$ is very similar to that of U and W in Fig.2. Here, the bracket $< >$ represents the average in the horizontal plane.

Figure 3 shows the distributions of the turbulence intensities and turbulence kinetic energy (TKE). In the vertical rotating open channel flow, since the Coriolis force induces the spanwise mean velocity, there exist both the streamwise and spanwise mean shear effects. Thus, the production of the streamwise velocity fluctuation comes from both processes. One is the shear process related to $< u >$, and the other is the splattering effect associated with $< w >$. So does the spanwise velocity fluctuation. As N_τ increases, the near-wall shear rate related to $< u >$ reduces significantly. Thus, a decrease of $< u'_{\rm rms} >$ is observed.

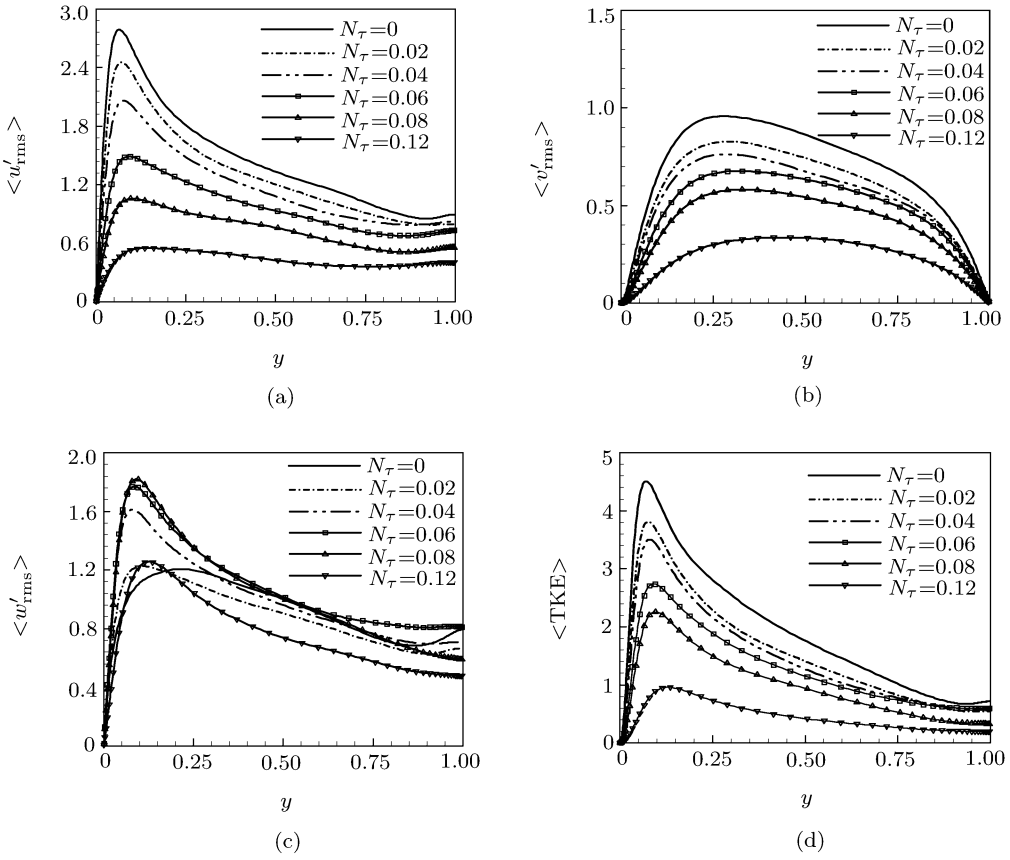


Fig.3. Distributions of turbulence intensities and turbulence kinetic energy: (a) streamwise, (b) vertical, (c) spanwise component, and (d) turbulence kinetic energy. Here, the bracket $< >$ represents the average in the horizontal plane in this and the following figures.

When N_τ varies from 0 to 0.06, the spanwise velocity fluctuation $< w'_{\rm rms} >$ is enhanced due to increase of the spanwise mean shear rate. When N_τ increases further, the turbulence fluctuation is suppressed by the effect of Coriolis force, which causes the reduction of three turbulence intensities. As for turbulence kinetic energy versus N_τ, $<$ TKE $>$ decreases monotonically because of the dominant role of $< u'_{\rm rms} >$ and $< v'_{\rm rms} >$. In addition, the turbulence intensities exhibit a strong anisotropy near the free surface.

Figure 4 shows the mean vorticity. The streamwise mean flow is responsible for the spanwise mean vorticity $< \omega_3 >$; the spanwise mean flow induced by the Coriolis force produces the streamwise mean vorticity $< \omega_1 >$. As N_τ increases, $< \omega_3 >$ decreases monotonically, while $< \omega_1 >$ increases when the rotation number increases to 0.06, then decreases gradually.

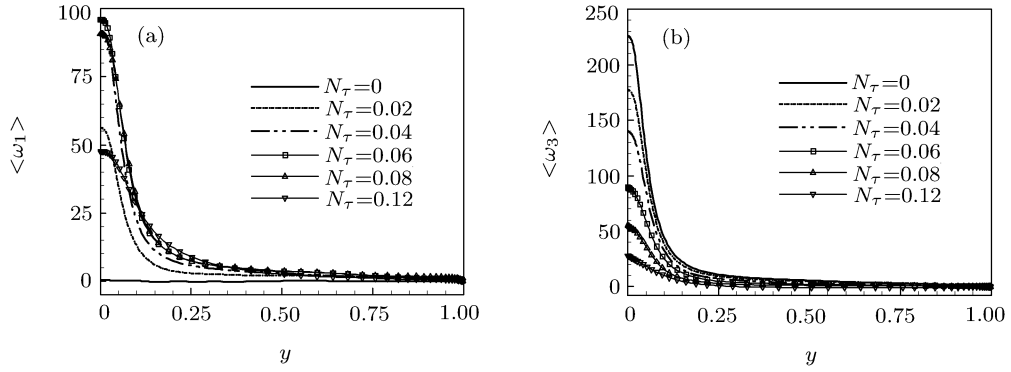


Fig.4. Profiles of the mean vorticities: (a) streamwise and (b) spanwise component.

4.2. Reynolds stress budgets

Figure 5 shows the budget terms in the streamwise Reynolds stress transport equation. In the viscous sublayer $y < 0.02$ ($y^+ < 4$), the budget is balanced mainly between viscous diffusion term (VD) and dissipation term (DS). In the region around $y = 0.06$

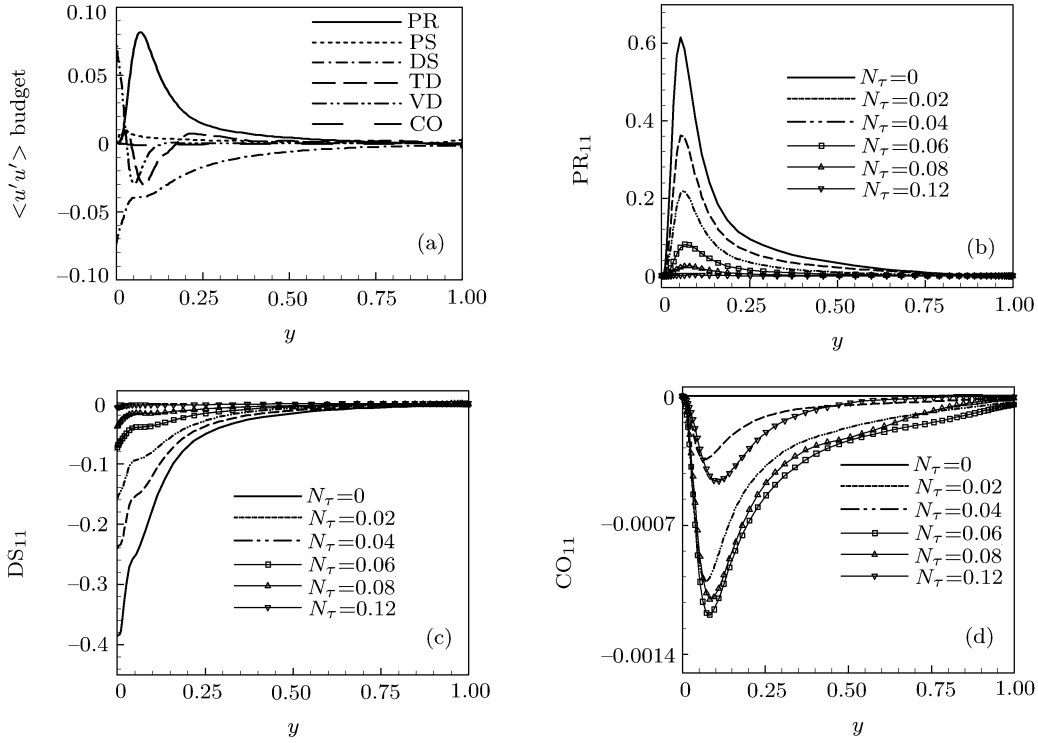


Fig.5. Distributions of the budget terms in the transport equation of $< u'u' >$: (a) budget terms at N_τ= 0.06, (b) production term, (c) dissipation term, (d) Coriolis force term.

($y^+ = 12$), production term (PR), dissipation term (DS), turbulence diffusion term (TD) and viscous diffusion term (VD) play as major contributions to the budget balance. In the near free surface region, all the terms become small. To elucidate the rotating effects, the profiles of some typical terms are shown in Figs.5(b)–5(d). In the rotating case, the non-zero Coriolis force budget term CO_{11} arises, however, it is negligibly small. With the increase of N_τ, the magnitudes of PR_{11} and DS_{11} decrease monotonically, while CO_{11} increases first and then decreases. Although the CO_{11} terms are relatively small, the Coriolis force actually plays a significant role on turbulence statistics.

As shown in Fig.3, the turbulence intensities have a strong anisotropy near the free surface. Analyses of the turbulence kinetic energy and dissipation budgets have revealed that anisotropic dissipation and pressure–strain effects are principally responsible for the anisotropy.[4,12] To exhibit the mechanism of strong anisotropy, the characteristics of the pressure–strain on the energy transfer near the free surface are discussed. The distributions of the pressure–strain terms are shown in Fig.6. The pressure–strain term in the vertical direction (PS_{22}) decreases significantly near the free surface and its sign changes from positive to negative, while those in the streamwise direction and spanwise direction (PS_{11} and PS_{33}) increase monotonically. Thus, the turbulence kinetic energy in the vertical direction is transferred into the spanwise and streamwise directions through the pressure–strain effect.

4.3. Flow structures

The structures of streamwise and spanwise velocity fluctuations in the (x, z) plane at $y^+ = 191.6$ (i.e., near the free surface) for three different rotation numbers are shown in Figs.7, respectively. Unlike the flow patterns near the bottom,[8] very long and smooth streaks do not exist near the free surface. It is consistent with the experimental observations.[1,2] As N_τ increases, the contours of streamwise velocity fluctuations become sparse monotonically, while those of spanwise velocity fluctuations become dense when the rotation number increases to 0.06, then become sparse gradually. The characteristics is in well agreement with the turbulence intensities in Figs.3(a) and 3(c).

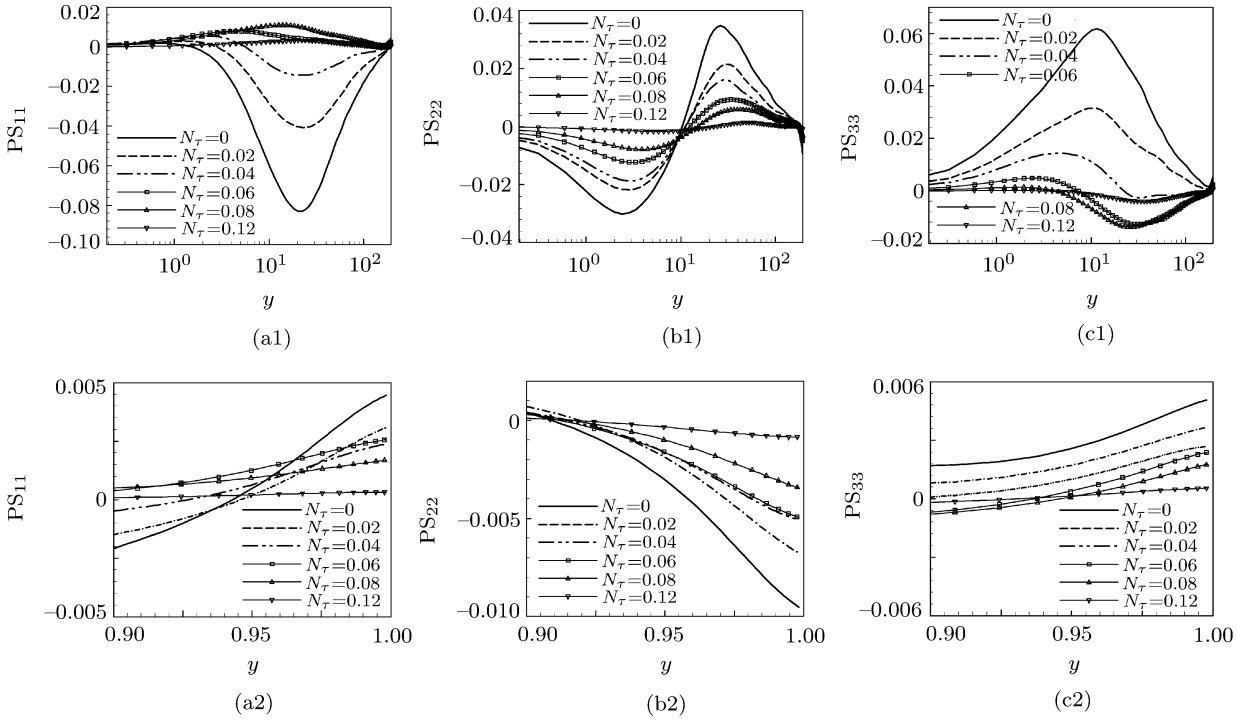


Fig.6. Distributions of the pressure–strain terms in the wall coordinate (upper) and near the free surface (bottom): (a) streamwise, (b) vertical, (c) spanwise component. Here, the wall coordinate y^+ is defined as $y^+ = y \times \mathrm{Re}_\tau$ in this and the following figures.

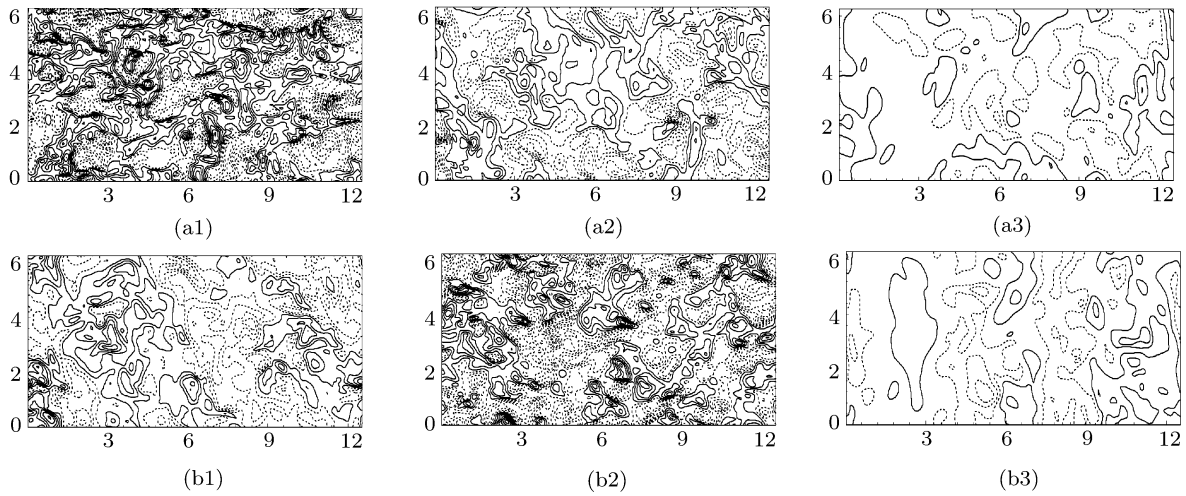


Fig.7. Contours of the instantaneous streamwise (upper) and spanwise (bottom) velocity fluctuations in a plane parallel to the wall at y^+=191.6: (1) $N_\tau = 0$, (2) $N_\tau = 0.06$, (3) $N_\tau = 0.12$. Here, solid lines represent positive values and dashed lines negative values. Increments of u' and w' are 0.8 and 0.4, respectively.

Based on experimental observations and numerical simulations,[1,2,13] the most surface renewal events are due to bursting processes near the solid boundary and are closely correlated with boundary layer bursts. Here, the patterns of streamwise velocity fluctuation in the (x, y) plane for three rotation numbers are shown in Fig.8. The well-known high-speed streaks (dense solid lines) are clearly illustrated. Moin and Kim[14] postulated that the wall layer may be viewed as a bed of low-speed fluid that is constantly subjected to the arrival of energetic eddies from the outer layers. These energetic eddies form the high-speed streaks in the wall region. Thus, as observed in Fig.8, the bursting processes near the bottom wall are ejected toward the free surface. When N_τ increases, the contours along the streamwise direction become sparse. It may be related to the significant role of Coriolis force on turbulence statistics and flow patterns for different rotation number. Meanwhile, the absent and healthy streaky structures obviously demonstrate the strength of velocity fluctuation in Figs.8, and are consistent with the distributions of the velocity fluctuation in Fig.3(a).

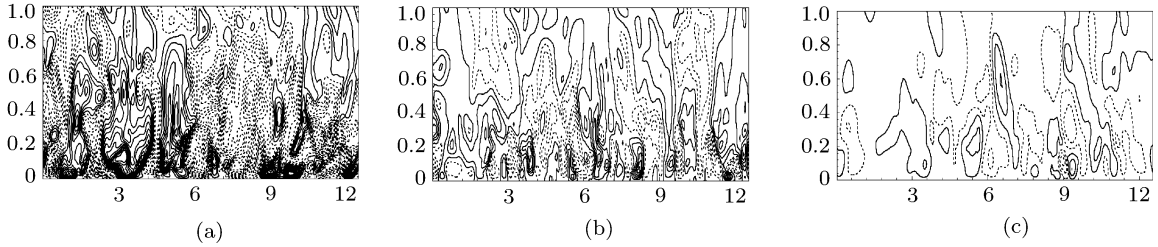


Fig.8. Contours of the instantaneous streamwise velocity fluctuations in the (x, y) plane: (a)$N_\tau = 0$, (b)$N_\tau = 0.06$, (c) $N_\tau = 0.12$. Here, solid lines represent positive values and dashed lines negative values. Increment of the contours is 1.

5. Concluding remarks

Direct numerical simulation is performed to investigate the behaviours of the vertical rotating open channel flow. Two typical rotation regimes are identified. One is weak rotation regime, the turbulence statistics relevant to the spanwise velocity fluctuation are augmented, but the other statistics are suppressed. The other is strong rotation regime, all the turbulence statistics decrease sharply. The budget of $< u'u' >$ exhibit the alteration of the mechanisms to generate the streamwise turbulence fluctuations. The profiles

of pressure–strain term elucidate that turbulence kinetic energy in the vertical direction is transferred into the spanwise and streamwise directions. The flow structures exhibit that the bursting processes near the bottom wall are ejected toward the surface. As N_τ increases, the contours of streamwise velocity fluctuations become sparse monotonically, while those of spanwise velocity fluctuations become dense first, and then become sparse gradually.

References

[1] Nakagawa H and Nezu I 1981 *J. Fluid Mech.* **104** 1

[2] Komori S, Murakami Y and Ueda H 1989 *J. Fluid Mech.* **203** 103

[3] Esau I 2003 *J. Turbulence* **4** 17

[4] Wang L, Dong Y H and Lu X Y 2005 *Comput. Fluids* **34** 23

[5] Orlandi P and Ebstein D 2000 *Int. J. Heat Fluid Flow* **21** 499

[6] Pan Y K, Tanaka T and Tsuji Y 2001 *Phys. Fluids* **13** 2320

[7] Zou L Y, Liu N S and Lu X Y 2006 *Comput. Fluids* **35** 74

[8] Li B Y, Liu N S and Lu X Y 2006 *Int. J. Heat Mass Transfer* **49** 1162

[9] Li B Y, Liu N S and Lu X Y 2006 *Commun. Comput. Phys.* **1** 332

[10] Bai J S, Li P, Zhang Z J, Hua J S and Tan H 2004 *Chin. Phys.* **13** 1992

[11] Bai J S, Zhang Z J, Li P and Zhong M 2006 *Chin. Phys.* **15** 22

[12] Perot B and Moin P 1995 *J. Fluid Mech.* **295** 199

[13] Guo H and Lian Q X 2004 *Acta Phys. Sin.* **53** 2226 (in Chinese)

[14] Moin P and Kim J 1982 *J. Fluid Mech.* **118** 341